 DOI: 10.1002/masy.200950514

# Shear-Induced Phase Separation of Entangled Polymer Solutions: Formation of Optically Anisotropic Strings as Precursor Structures of Shish-Kebab

*Takeji Hashimoto,*[*1] *Hiroki Murase,*[2] *Yasuo Ohta*[2]

**Summary:** Shear-induced structures were investigated for both ultrahigh molecular weight atactic polystyrene (UHMWaPS) and linear polyethylene (UHMWPE) solutions, which were entangled but homogeneous without shear flow, as a function of shear rate ($\dot{\gamma}$) or time after a step-up shear flow. For the PE solutions, the shear flow was imposed at 124 °C which is higher than the nominal melting temperature $T_{nm}$ of the solution without shear flow. At sufficiently high shear rates both solutions commonly formed highly optically anisotropic string-like structures which are composed of a series of phase-separated domains interconnected by bundles of stretched chains and aligned along the flow direction. After cessation of the shear flow the string-like structures completely disappeared in the UHMWaPS solution, recovering a homogeneous solution, while the UHMWPE solution exhibited shish-kebab structure. The results reveal a new kinetic pathway for shish-kebab formation for the entangled crystallizable solution sheared at $T > T_{nm}$ which involves first formation of the phase-separated string-like domains and subsequent crystallization into shish from the bundles of stretched chain and then kebab in the demixed domains composed of essentially random coils.

**Keywords:** crystallization; phase separation; rheo-optics; semidilute polymer solutions; shear flow; shish-kebab

## Introduction

Studies of ordered structures (the sol-called dissipative structures) of soft matters under external fields are believed to be important basic research subjects in statistical mechanics on open non-equilibrium phenomena.[1] In this work, we shall focus on entangled solutions of ultrahigh molecular weight atactic polystyrene (UHMWaPS) and polyethylene (UHMWPE) as a model for noncrystallizable and crystallizable solution, respectively. Generally these solutions belong to dynamically asymmetric systems[1–5] where the components of systems, polymer and solvent in this case, have a large difference in self-diffusivity. The systems can be considered to be an extreme case of binary polymer blends having a large molecular weight difference in their constituent components. For simplicity, the solutions to be studied in this work are restricted to those in thermodynamically stable ones, hence homogeneous solutions involving no liquid-liquid phase separation and crystallization in the absence of shear flow. However, the homogeneous solutions become unstable under shear and undergo phase separation due to the viscoelastic effect[6–9] or crystallization due to chain orientation.

We shall discuss the following shear-induced structures for the homogeneous solutions in the quiescent state: (i) shear-induced phase separation, (ii) formation of

[1] Advanced Science Research Center, Japan Atomic Energy Agency, Tokai, Naka-gun, Ibaraki 319-1195, and Department of Polymer Chemistry, Kyoto University, Kyoto 615-8510, Japan
E-mail: hashimoto@alloy.polym.kyoto-u.ac.jp
[2] TOYOBO Co., Ltd., Research Center, 2-1-1, Katata, Ohtsu-shi, Shiga 520-092, Japan

string-like structures, i.e., nematically aligned phase-separated domains along the flow direction at high shear rates, and (iii) a sharp transition of optical properties of the strings, with further increasing shear rates, from a state having a small oprical anisotropy to that having a large optical anisotropy. The transition implies formation of bundles of stretched chains interconnecting the domains within the string. We shall elucidate that, interestingly enough, these results (i) to (iii) are observed ''commonly'' for both the noncrystallizable and crystallizable solutions. In the case of the crystallizable solutions, the strong optical anisotropy does remain even after cessation of shear flow, which provides an important piece of information to understand formation of precursor structures of shish-kebabs.[10–13]

## Experimental Part

The shear-induced structure formation was explored by the rheo-optical apparatuses constructed in our laboratory[14–16] which enable simultaneous observations of small-angle light scattering (shear-SALS), optical microscopy (shear-OM), birefringence, and stress under various shear flow fields. Typical UHMWaPS used had $M_w = 5.48 \times 10^6$ and $M_w/M_n = 1.15$, while UHMWPE had $M_w = 2.0 \times 10^6$ and $M_w/M_n = 12$. The typical entangled solutions studied had concentration = 6.0 wt% in dioctylphthalate (DOP) for UHMWaPS ($c/c^* = 40$) and 5.0 wt% in paraffin having melting temperature $T_m$, $T_m = 69\,^\circ C$ and $M_n \sim 500$ ($c/c^* = 11$) where $c^*$ is the overlap concentration.

The UHMWPE was mixed in the paraffin wax with an antioxidant agent (2,6-di-*tert*-butyl-*p*-cresol), by an amount of 1 wt % of the total solution, using a screw-type extruder at 210 °C. Small particles contaminating the solutions were filtered off by a mesh filter (400 lines/in.). This process is very important to obtain good scattering data.[17] If we omit this process, intense scattering arising from the particles will disturb the genuine light scattering from the semidilute solutions.

## Results and Discussion

Figure 1 typically shows some properties under steady-state shear flow as a function of shear rate $\dot{\gamma}$ for a 6.0 wt% solution of the UHMWaPS ($M_w = 3.84 \times 10^6$, $M_w/M_n = 1.06$, $c/c^* \approx 30$) in DOP at 21 °C[18]: part *a* presents viscosity $\eta$, birefringence $\Delta n'$, and form dichroism $\Delta n''$; part *b* presents the normalized integrated scattered intensities parallel (//) and perpendicular ($\perp$) to the flow direction; part *c* presents isointensity contour plots of the scattering patterns. The steady-state behaviors of these properties are classified into four regimes (Regime I to IV) as shown in part *a* with respect to three characteristic shear rates $\dot{\gamma}_{c,x}$, $\dot{\gamma}_{c,z}$, and $\dot{\gamma}_a$[1,19] as will be defined later in conjunction with Figure 3.

Figure 2 typically shows time evolution of the normalized integrated scattered intensity parallel (//) and perpendicular ($\perp$) to the flow direction (part *a*) and birefringence (part *b*) after a step-up shear from $\dot{\gamma} = 0$ to $\dot{\gamma} = 2.9\ s^{-1} > \dot{\gamma}_a (= 1.2\ s^{-1})$ for the 5.0 wt% crystallizable UHMWPE in paraffin at 124 °C above $T_{nm} = 115$–120 °C, the nominal melting temperature of the solution in the quiescent state.[20] The transient behaviors of these properties are also classified into four regimes (Regime I to IV) with respect to three characteristic times $t_{c1}$, $t_{c2}$, and $t_{c3}$ or shear strains $\dot{\gamma}_{c1}$, $\dot{\gamma}_{c2}$, and $\dot{\gamma}_{c3}$, as will be also defined below in conjunction with Figure 3. The transient behaviors of the noncrystallizable UHMWaPS also are quite similar to those of UHMWPE.[1,21]

Figure 3 summarizes the results shown in Figures 1 and 2 and expected dissipative structures formed under steady or step-up shear flow, *commonly found for the noncrystallizable and crystallizable entangled solutions*. Upon increasing $\dot{\gamma}$ under steady shear or time $t$ after the step-up shear from $\dot{\gamma} = 0$ to $\dot{\gamma} > \dot{\gamma}_a$, the critical shear rate for an onset of the anomaly to be described later

 

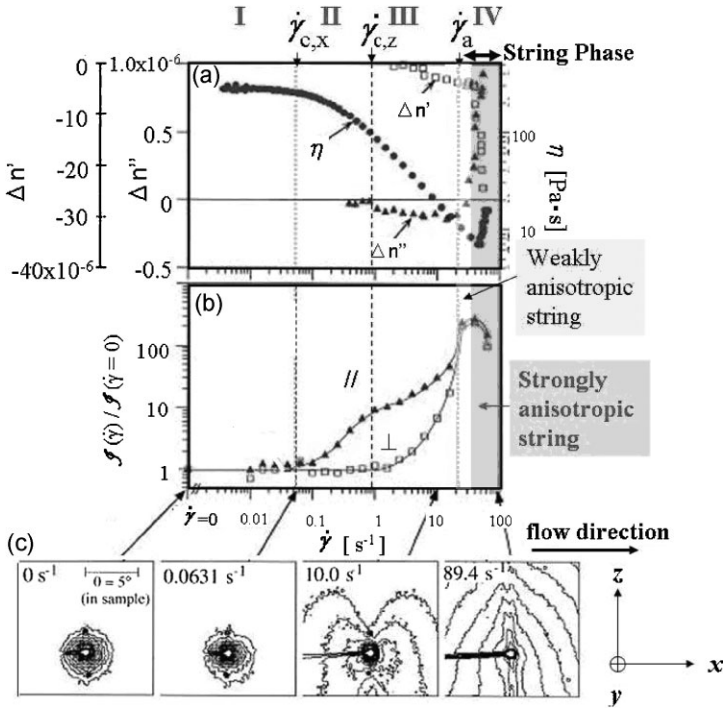


***Figure 1.***

Shear-rate ($\dot{\gamma}$) dependence of various quantities for a 6.0 wt% solution of UHMWaPS at 21 °C: (a) Birefringence $\Delta n'$, form dichroism $\Delta n''$, and viscosity $\eta$: (b) normalized integrated intensity parallel (//) and perpendicular ($\perp$) to the flow direction; (c) isointensity contour plots of SALS patterns in *Oxz* plane where the *x*-, *y*-, and *z*-axis are taken parallel to the flow direction, velocity-gradient direction, and neutral (or vorticity) direction, respectively.

[see top row (A)], shear-SALS patterns (schematics), contrast-enhanced transmission shear-OM images, and rheological properties undergo the characteristic changes as shown in row (B), (C), and (D), respectively. The corresponding changes in the dissipative structures are summarized in row (E). All the patterns shown in row (B) and (C) are taken in *Oxz* plane where the flow, velocity gradient, and neutral (or vorticity) directions are commonly set parallel to *x*, *y*, and *z* axis, respectively.

The rheo-optical behaviors are classified into the following four regimes:

– **Regime** I where $\dot{\gamma} < \dot{\gamma}_{c,x}$ or $t < t_{c1}$ (corresponding to the terminal rheological relaxation time). The solutions are homogeneous even under the shear flow as in the quiescent solution (see the data at $\dot{\gamma} < \dot{\gamma}_{c,x}$ in Figure 1 a–c) and in the incubation time for the shear-induced structure formation (see the data at $t < t_{c1}$ in Figure 2).
– **Regime II** where $\dot{\gamma}_{c,x} < \dot{\gamma} < \dot{\gamma}_{c,z}$ or $t_{c1} < t < t_{c2}$. Shear enhances plane-wave type concentration fluctuations with their wave vectors preferentially oriented along the *x* axis but does not affect much the fluctuations along the *z* axis, giving rise to the characteristic butterfly patterns with the dark streak along the z axis. (Figure 1b, 2a, and 3b in row (B)).[19,22]
– **Regime III** where $\dot{\gamma}_{c,z} < \dot{\gamma} < \dot{\gamma}_a$ or $t_{c2} < t < t_{c3}$, and $\dot{\gamma}_a$ approximately corresponds to $\tau_e^{-1}$ where $\tau_e$ is the rheological relaxation time for chain stretching. The scattering along the neutral axis starts to remarkably increase (Figure 1b and 2a), which may be a signature of a transformation from the shear-enhanced plane-wave type concentration fluctuations to shear-induced demixed structures.[1,23–25] Judging from the shape

 

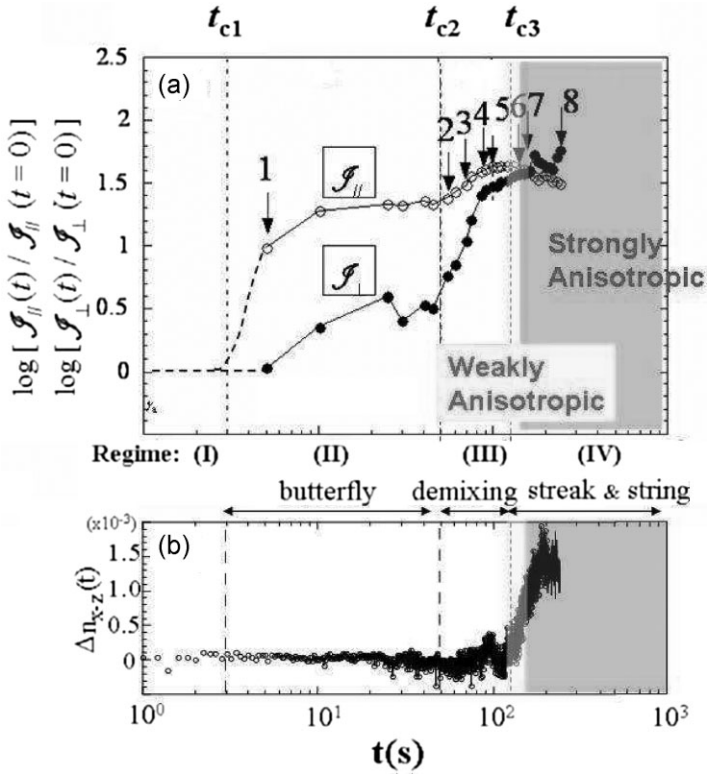


***Figure 2.***
Time evolutions of normalized integrated intensity parallel (//) and perpendicular (⊥) to the flow direction (a) and birefringence $\Delta n_{xz}$ (b) after a step-up shear flow from $\dot{\gamma} = 0$ to $\dot{\gamma} = 2.9\ s^{-1} > \dot{\gamma}_a = 1.2\ s^{-1}$ for the 5.0 wt% UHMWPE solution at 124 °C.

of the butterfly pattern, the demixed domains extend along $z$ axis but compressed along $x$ axis as schematically shown in part (c′) in row (C) in Figure 3. Their centers of mass are randomly aligned along the $z$ axis as illustrated in part (c′) in row (C) and as actually shown by the OM images in part (c) in row (C) in Figure 3.[15,17,26,27] Rheology exhibits the shear thinning in Regime II and III (Figure 1a).[18,19,21,28–30] The sheared solutions show almost no birefringence up to Regime III (Figure 1a, 2b), indicating that polymer chains are essentially in relaxed random coils even under the shear flow.

– **Regime IV** where $\dot{\gamma} > \dot{\gamma}_a$ or $t > t_{c3}$. The sharp streak-like scattering pattern with strong intensity appears along the $z$ axis (Figure 1c).[18,20,21,31] The streak pattern is superposed on the butterfly pattern as shown actually in the pattern at $\dot{\gamma} = 89.4\ s^{-1}$ in Figure 1c and schematically in part (d), row (B) in Figure 3. This implies that the demixed domains tend to align into string-like structures oriented parallel to flow as schematically shown in part (d′), row (C) in Figure 3. The string as a whole [as shown in part (d), row (C) in Figure 3] gives rise to the streak pattern, while the domain structures within the strings [as schematically shown in part (d′), row (C) in Figure 3] give rise to the butterfly pattern. The domains structures within the strings could not be clearly resolved by the shear OM for the case of UHMWaPS solutions as shown in part (d), row (C) in Figure 3,[28] though they were identified in the case of the UHMWPE solutions.[20,31] The

 

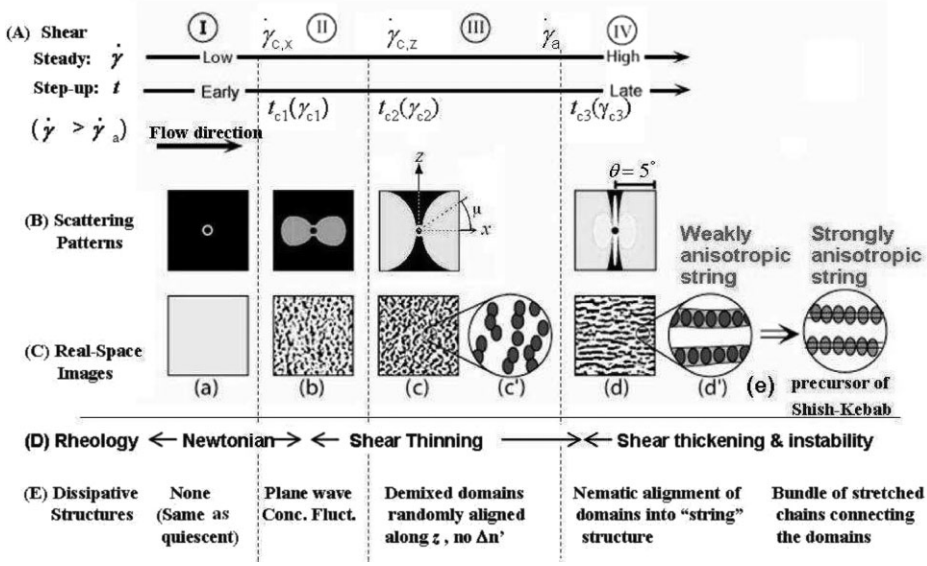


***Figure 3.***
Structures formed under steady-state shear flow and time-evolution of transient structures formed after imposing a step-up shear flow from zero shear rate to a given $\dot{\gamma}$ greater than $\dot{\gamma}_a$. A set of data shown in row (B) to (E) is meant to represent the steady-state and transient structures or properties developed in each regime show in column (a) to (d). $\gamma_{ci}$ (i = 1, 2, or 3) is total strain defined by $\gamma_{ci} = \dot{\gamma} t_{ci}$.

nematic alignment of the demixed domains into the strings may be due to hydrodynamic effects. The strings have only a weak birefringence ($\Delta n'$ in Figure 1a and $\Delta n_{xz}$ in Figure 2b) in the beginning of Regime IV. Upon further increasing $\dot{\gamma}$ or $t$, $|\Delta n'|$or $\Delta n_{xz}$ suddenly starts to increase (Figure 1a and Figure 2b),[1,18,20] indicating a sharp transformation from weakly anisotropic strings to strongly anisotropic strings. This transformation may imply formation of bundles of stretched chains connecting the nematically aligned domains as schematically shown in part (e) in row (C) in Figure 3.[20] The transformation is accompanied by the shear thickening (Figure 1a) and instabilities in shear stress and the first normal stress difference.[18,20,21] The large fluctuations (oscillation) of $\Delta n_{xz}$, especially in Regime IV, may reflect the stress instability caused by repeated stretching and relaxation of chains.

On-line and real-time observations of the SALS patterns at the given temperatures after the cessation of shear revealed that: (a) the streak-like pattern totally disappeared in the case of the noncrystallizable UHMWaPS solutions in the order of 200 s; (b) On the contrary it increased the scattered intensity in the case of the UHMWPE solutions.[20,31] This implies that the UHMWaPS solutions containing the optically anisotropic strings relax back to homogeneous solutions, because there are no solidification mechanisms for the strings in the solutions. On the other hand, in the case of the UHMWPE solutions at 124 °C, even after the cessation of shear, the strings did not decay but rather grow, probably due to further crystallization of the strings, which serves as a solidification mechanism, as evidenced by the increase of the scattered intensity of the streak.[20,31]

The UHMWPE solution after cessation of the imposed shear at $\dot{\gamma} = 2.9\ s^{-1}$ for 130s at 124 °C was rapidly cooled down below $T_m$ of paraffin in the time scale of roughly about 10s by soaking the specimen in between the cone-and-plate fixture made out of cooper into liquid nitrogen in order

 

to solidify the specimen for investagation of the structures developed in the solution under transmission electron microscopy (TEM). For TEM observation, a small piece of the sample was cut out from the solidified solution with a recognition of the *Oxyz* coordinate from the sample shape and from the cutting directions. The sample was then immersed in a liquid paraffin at 79 °C above $T_m$ of the paraffin used as a solvent under a gentle agitation for 1h in order to exchange paraffin to noncrystallizable liquid paraffin. The liquid paraffin was then replaced stepwisely by propylene oxide from liquid paraffin/propyleneoxide with 100/0 wt/wt to 50/50 wt/wt for 30 min., to 25/75 wt/wt for15 hrs and to 0/100 wt/wt for 1 h; The last step was repeated five times. Then propylene oxide also was stepwisely replaced by epoxy monomer from propylene oxide/epoxy monomer with 100/0 wt/wt to 50/50, 25/75, and 0/100 wt/wt with each step for 15 hrs; The last step was repeated three times. The specimen replaced by epoxy monomer was solidified by curing the monomer into the resin at 60 °C for 15 hrs.

The solidified specimen was trimmed to expose the inner region of the specimen to $RuO_4$ vapor for 10 hrs at room temperature for staining the specimen with $RuO_4$. Thus stained specimen was cut into ultrathin sections, with a diamond knife mounted on an ultramicrotone (Ultratome V, LKB, Co., Ltd., Stockholm, Sweden) at room temperature, into thickness of 70 nm parallel to the *Oxy* plane (the plane parallel to the velocity gradient and flow directions). The ultra-thin sections were mounted on carbon-coated polymer films [poly(vinyl formal)] on copper grids. TEM observation was carried out with JEM-2010CX (JEOL, Tokyo, Japan).

Figure 4 demonstrates a typical TEM observed after the processes involving the solvent replacements and the solidification of the UHMPE solutions. The TEM image clearly show the shish-kebab structures oriented parallel to the flow direction in the plane of the velocity gradient and flow directions. Since the image is obtained off-line after the series of the processes involving the cessation of shear, cooling down the solution to room temperature, the solvent replacements, and the solidification, the image would not strictly reflect the string structures existed on-line under shear at 124 °C. The string structures at 124 °C are well expected to be subjected further crystallization in the processes encountered by the cessation of the shear and cooling down bleow $T_{nm}$ of the UHMWPE solution. The crystallization occuring in these processes may involve nucleation and growth (NG) of shish from the bundles of stretched chains in the string and the lamellar overgrowth into kebabs from the shish within the demixed domains in the strings. We note that the NG of shish and lamellar overgrowth may occur even in relaxed melts as long as the melt exposed to the seeds of shishs through the ''autocatalitic process'' as reported by Petermann and coworkers.[32,33] In the light of the work by Petermann and coworkers, it is conceivable that the shish-kebab will be nucleated and grown from the string structures created at 124 °C even after shear cessation and during the series of the processes to prepare the specimen for TEM observation. Therefore the string structures developed in the UHMWPE solution at 124 °C are believed to serve as precursors for the shish-kebab formation.

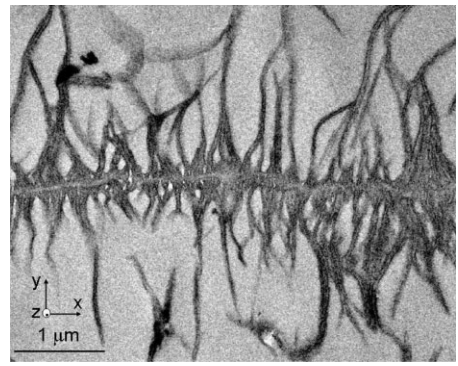


***Figure 4.***
Transmission electron micrograph demonstrating a shish-kebab structure developed from the 5.0 wt% UHMWPE solution under the shear flow in Regime IV.

 

## Concluding Remarks

In the past, the flow-induced NG of shish in dilute, semidilute, and concentrated solutions has been considered as a consequence of formation of bundles of stretched chains in homogeneous solution,[10–12,34,35] as schematically shown by a series of kinetic pathway from part (a) to (d) in Figure 5 for entangled crytallizable homogeneous solutions. The coils adhered to shishs are proposed to crystallize into lamellae and the lamellar overgrowth from the shishs results in the kebabs.

Our results on sheared entangled solutions elucidated a quite different kinetic pathway for the shear-induced crystallization into the shish-kebab structure. Upon imposing shear flow with $\dot{\gamma} > \dot{\gamma}_a$ to the homogeneous quiescent solution, the shear induced first (i) the plane-wave concentration fluctuations with their wave vectors preferentially oriented along the flow direction mediated by the elastic effects,[6–9] followed by transformation into (ii) demixed domains rich in random coils with their center of mass randomly arranged along their neutral axis. Upon a further elapse of time, (iii) centers of the domains are aligned nematically along the flow direction to result in formation of the string structures as shown in Figure 5(e) and (f), where the demixed domains are composed of entangled random coils. There may be some stretched chains which interconnect the domains, but the strings have only a small birefringence in the beginning. The process (iii) is expected to be dirven by hydrodynamic effects. The string undergoes a sharp transition from a weak birefringence to a strong birefringence as schematially shown from Figure 5(f) to (g), seemingly indicating (iv) formation of bundles of stretched chains interconnecting the demixed domains, which are still composed of random coils, as depicted in Figure 5(g).

The models shown in Figure 5(b) and 5(g) are different from each other with respect to nonexistence and existence of the demixed domains around the boundles of stretched chains, respectively. The difference reflects the different mechanism of formation of the bundles of the stretched chains: one from a homogeneous solution as shown in the part (a) to (b) and the other from the nematically aligned domains as shown in the parts (a) to (e) and then (e) to (g). We like to emphasize here that the working temperature $T$ is very important. In this work we deliberately chose $T = 124\,^{\circ}\mathrm{C} > T_{nm}$ (115–120 °C) so that the

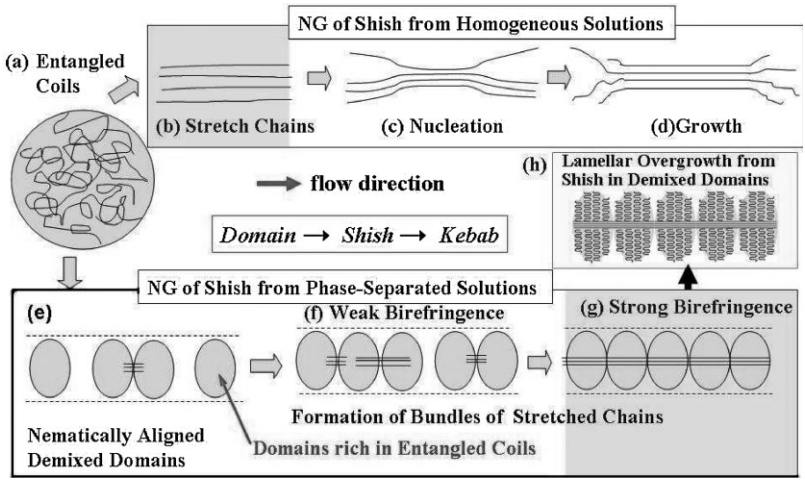


***Figure 5.***
Model showing nucleation and growth of shish from homogeneous entangled solutions (parts *a* to *d*) and from phase-separated domains (parts *a* to *e* and then *e* to *g*).

 

solutions without shear are homogeneous and stable for both liquid-liquid phase separation and crystallization. Imposing shear flow first induces the phase separation and then crystallization. If the working temperature is close to or lower than $T_{nm}$, the effects of shear on structure formation depend on initial states of the solutions, with respect to crystallization before the application of shear flow. Even in the case where the solutions are initially homogeneous, the shear-induced structure formation will be more complex than that at $T > T_{nm}$, because the two kinds of phase transitions induced by shear is expected to couple to each other in complex manners.

Back to the model shown in Figure 5(g), once NG of the shish occurs from the bundle of stretched chains, it induces the overgrowth of folded chain lamellae from entangled random coils in the demixed domains. The kinetic pathway, which evolves first demixed ''domains'', then ''shishs'' and finally ''kebabs'' with increasing strain, seems to form naturally a prototype structure of the shish-kebab, as schematically shown in Figure 5(h). The kinetic path involved in this work built up the domain period $\sim$10 μm and the lamellar spacing $\sim$10 nm. The lamellar overgrowth from shish occurs in a confined space of demixed domains, and hence the kebabs keep the memory of the shape of demixed domains.[36] However fractures and reformation of the prototype structures as well as long-range rearrangements of UHMPE molecules within the structures under shear flow will eventually erase the shape memory, yielding typical shish-kebab structures as reported in the past.

[1] T. Hashimoto, *Bull. Chem. Soc. Jpn.* **2005**, *78*, 1–39.
[2] M. Doi, A. Onuki, *J Physique* **1992**, *25*, 1631.
[3] H. Tanaka, *Macromolecules* **1992**, *25*, 6377.
[4] A. Onuki, *Non-Crystalline Solids* **1994**, *172*, 1151.
[5] A. Onuki, *Phase Transition Dynamics*, Cambridge Univ. Press, Cambridge, U.K 2002.
[6] E. Helfand, G. H. Fredrickson, *Phys. Rev. Lett.* **1989**, *62*, 2468.
[7] S. T. Milner, *Phys. Rev. E.* **1993**, *48*, 3774.
[8] A. Onuki, *Phys. Rev. Lett.* **1989**, *62*, 2472.
[9] A. Onuki, *J. Phys.: Condense Matter* **1997**, *9*, 6119.
[10] A. J. Penning, A. M. Kiel, *Kolliod ZZ Polym.* **1965**, *205*, 160.
[11] A. J. Penning, J. M. A. A. van der Mark, H. C. Booij, *Kolloid ZZ Polym.* **1969**, *236*, 99.
[12] A. Keller, H. W. H. Kolnaar, *Processing of Polymers*, Vol. *16*, H. E. H. Meijer, Ed., VCH, New York **1997**, p. 189.
[13] H. Somani, L. Yang, L. Zhu, B. S. Hsiao, *Polymer* **2005**, *46*, 8587.
[14] T. Hashimoto, T. Takebe, S. Suehiro, *Polymer J.* **1986**, *18*, 123.
[15] T. Kume, K. Asakawa, E. Moses, K. Matsuzaka, T. Hashimoto, *Acta Polym.* **1995**, *46*, 79.
[16] K. Matsuzaka, T. Hashimoto, *Rev. Sci. Instr.* **1999**, *70*, 2387.
[17] H. Murase, T. Kume, T. Hashimoto, Y. Ohta, T. Mizukami, *Macromolecules* **1995**, *28*, 7724.
[18] T. Kume, T. Hashimoto, T. Takahashi, G. G. Fuller, *Macromolecules* **1997**, *30*, 7232.
[19] T. Hashimoto, T. Kume, *J. Phys. Soc. Jpn.* **1992**, *61*, 1839.
[20] H. Murase, T. Kume, T. Hashimoto, Y. Ohta, *Macromolecules* **2005**, *38*, 8719.
[21] T. Kume, T. Hattori, T. Hashimoto, *Macromolecules* **1997**, *30*, 427.
[22] T. Hashimoto, K. Fujioka, *J. Phys. Soc. Jpn.* **1991**, *60*, 356.
[23] S. Saito, T. Hashimoto, I. Morfin, P. Lindner, F. Boue, *Macromolecules* **2002**, *35*, 445.
[24] S. Saito, T. Hashimoto, *J. Chem. Phys.* **2001**, *114*, 10531.
[25] I. Morfin, P. Lindner, F. Boue, *Macromolecules* **1999**, *32*, 7208.
[26] E. Moses, T. Kume, T. Hashimoto, *Phys. Rev. Lett.* **1994**, *72*, 2037.
[27] H. Murase, T. Kume, T. Hashimoto, *Macromol. Symp.* **1996**, *104*, 159.
[28] T. Kume, T. Hashimoto, *ACS Symp. Series* **1995**, *597*, 35.
[29] M. K. Endoh, S. Saito, T. Hashimoto, *Macromolecules* **2002**, *35*, 7692.
[30] M. K. Endoh, M. Takenaka, T. Hashimoto, T. Inoue, H. Watanabe, *J. Chem. Phys.* **2008**, *128*, 164911.
[31] H. Murase, T. Kume, T. Hahsimoto, Y. Ohta, *Macromolecules* **2005**, *38*, 6656.
[32] J. Petermann, M. Miles, H. Gleiter, *J. Polym. Sci: Polym. Phys. Ed.* **1979**, *17*, 55.
[33] I. Liberwirth, J. Loos, J. Petermann, A. Keller, *J. Polym. Sci.: Part B: Polym. Phys.* **2000**, *38*, 1183.
[34] J. D. Foffmann, *Polymer* **1979**, *20*, 701.
[35] I. Dukovski, M. Muthukumar, *J. Chem. Phys.* **2003**, *118*, 6648.
[36] H. Murase, Y. Ohta, T. Hashimoto, paper in preparation.

 